



Pergamon

J. Mech. Phys. Solids, Vol. 46, No. 10, pp. 1997–2016, 1998

© 1998 Elsevier Science Ltd. All rights reserved

Printed in Great Britain

0022-5096/98 \$—see front matter

PII: S0022-5096(98)00035-0

DYNAMIC CRACK INITIATION IN DUCTILE STEELS

P. R. GUDURU, R. P. SINGH, G. RAVICHANDRAN and A. J. ROSAKIS†

Graduate Aeronautical Laboratories, California Institute of Technology, Pasadena CA 91125, U.S.A.

(Received 20 December 1997; in revised form 13 February 1998)

ABSTRACT

The goal of the work presented here is to study dynamic crack initiation in ductile steels (Ni–Cr steel and 304 stainless steel) at different loading rates and to establish appropriate dynamic failure criteria. A variety of infrared and visible optical methods and high-speed photography are used in this study. Precracked steel specimens are subjected to dynamic three-point bend loading by impacting them in a drop weight tower. During the dynamic deformation and fracture initiation process the time history of the transient temperature in the vicinity of the crack tip is recorded experimentally using a high-speed infrared detector. The dynamic temperature trace in conjunction with the HRR solution is used to determine the time history of the dynamic J -integral $J^d(t)$, and to establish the dynamic fracture initiation toughness, J_c^d . The measurements made using high-speed thermography are validated through comparison with determination of $J^d(t)$ by dynamic optical measurements of the crack tip opening displacement (CTOD). Finally, the micromechanisms of fracture initiation are investigated by studying the fracture surface using scanning electron microscopy. © 1998 Elsevier Science Ltd. All rights reserved.

Keywords: A. fracture toughness, dynamic fracture, B. elastic–plastic material, C. electron microscopy

1. INTRODUCTION

To aid in the design and vulnerability analysis of impact loaded structures and energy systems (e.g., pressure vessels, pipelines and reactors), it is necessary to quantify the mechanical behavior and failure modes of materials used in such systems under carefully controlled conditions. Because of design constraints and safety issues, these energy systems are typically fabricated with corrosion resistant and highly ductile metallic alloys such as stainless and Ni–Cr steels. Yet, relatively little is known regarding dynamic crack initiation and growth in such ductile metals. A major stumbling block in this area is the measurement of relevant fracture parameters, such as the J -integral, under a combination of large scale yielding conditions and dynamic loading. Considerable effort has been made towards the analytical and computational characterization of fracture parameters in highly ductile metals (Hutchinson, 1968; Rice and Rosengren, 1968; Needleman and Tvergaard, 1987; Nakamura and Parks, 1990; Narasimhan and Rosakis, 1990; Duffy and Chi, 1992; Cho *et al.*, 1993). Recently, several researchers have presented detailed analyses of ductile fracture using higher order expansions of the deformation fields within the plastic zone (Li and

† To whom correspondence should be addressed. Tel.: 626 395 3690. Fax: 626 449 2677. E-mail: rosakis@atlantis.caltech.edu

Wang, 1986; Sharma and Aravas, 1991; O'Dowd and Shih, 1991, 1992; Yang *et al.*, 1993).

To date relatively little experimental work has been done on determining fracture parameters, such as $J^d(t)$, for ductile fracture under dynamic loading conditions. Limited cases exist where careful choice of specimen geometry and loading histories allow for the measurement of J^d based on the use of dynamic boundary value measurements interpreted on the basis of quasi-static formulae for J (Costin *et al.*, 1977). Also, Douglas and Suh (1988) and Sharpe *et al.* (1988) have developed an alternate method based on comparing a dynamic finite element analysis with experimental observations to provide the critical value of CTOD (crack tip opening displacement) and thus the critical value of J , corresponding to crack initiation. The only direct measurements of the dynamic value of the J -integral, $J^d(t)$, have been made using the optical technique of caustics in conjunction with high-speed photography (Rosakis *et al.*, 1988; Zehnder *et al.*, 1990). However, even this approach employs a procedure using calibration of J vs the caustic diameter, D , under quasi-static loading conditions and then extends the same to dynamic loading conditions. Hence, this technique is limited to rate-insensitive materials and requires calibration for all combinations of specimen material and specimen geometry.

The current study introduces a technique for measurement of temperature variation in the vicinity of the dynamically loaded crack tip using a high speed infrared detector to determine the time history of the dynamic value of the J -integral, $J^d(t)$. The dynamic temperature trace is also employed to establish the dynamic fracture initiation toughness, $J^d(t_c) = J_t^d$, where t_c is the time of fracture initiation. The measurements made using high-speed thermography are validated through comparison with determination of $J^d(t)$ by dynamic optical measurements of the crack tip opening displacement (CTOD). Both these techniques provide a direct measurement of the time history of the dynamic J -integral and are not restricted by specimen geometry, rate of loading, or rate-sensitivity of the material.

2. EXPERIMENTAL SETUP

In this investigation high-speed infrared measurements of temperature and optical measurements of crack tip opening displacements were employed to study dynamic crack initiation in precracked ductile steel specimens. In the former, the temperature increase ahead of the crack tip during dynamic deformation is measured and is related to the dynamic J -integral. In the latter, the dynamic J -integral is estimated by relating it to the measured crack opening displacement history.

2.1. Specimen configuration, loading arrangement and material properties

The experiments employed edge cracked specimens in a three point bend configuration. The specimens were fabricated out of 2.3Ni–1.3Cr steel (will be referred to as Ni–Cr steel here onwards) and 304 stainless steel, whose compositions are listed

Table 1. Composition for Ni-Cr steel and 304 stainless steel

	C	Mn	Cu	Si	Ni	Cr	Mo	Co
Ni-Cr	0.17	0.30	0.13	0.22	2.35	1.32	0.25	—
304 Stainless	0.024	1.77	0.28	0.33	8.16	18.33	0.35	0.1

Table 2. Material properties for Ni-Cr steel and 304 stainless steel

Properties	Ni-Cr	304 Stainless
Young's modulus, E (GPa)	205	193
Density, ρ (kg/m ³)	7910	7900
Specific heat, c_p (J/Kg-K)	460	500
Yield Stress, σ_0 (MPa) ($\dot{\epsilon} = 10^{-3} \text{ s}^{-1}$)	750	510
Hardening exponent, n ($\dot{\epsilon} = 10^{-3} \text{ s}^{-1}$)	8	7

in Table 1. The relevant material properties for these two steels are listed in Table 2. Both the steels are relatively low to medium strength steels and fail in a ductile fashion under the given test conditions. Ni-Cr steel is strain rate sensitive as demonstrated by the uniaxial compression stress-strain behavior shown in Fig. 1. There was a significant elevation in the yield stress, σ_0 , as the strain rate was increased from 10^{-3} –

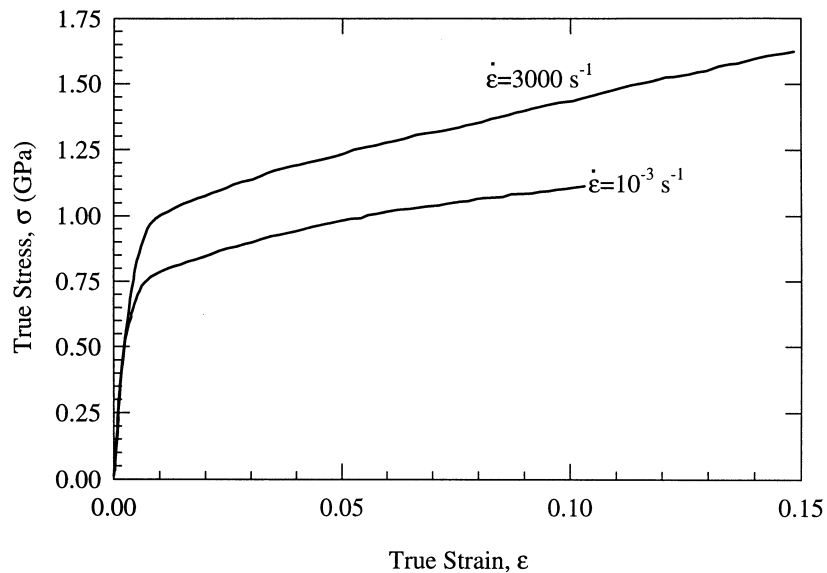


Fig. 1. Stress-strain behavior for Ni-Cr steel under uniaxial compression.

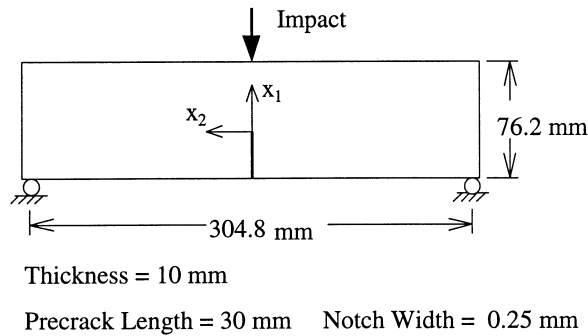


Fig. 2. Schematic of three-point bend impact loading of a precracked steel specimen.

10^3 s^{-1} . However, no appreciable change in the hardening exponent, n , was observed. On the other hand, 304 stainless steel is relatively rate insensitive and does not demonstrate any appreciable change in yield properties for the same change in strain rate. Dimensions for the edge-cracked specimen are shown in Fig. 2. An initial crack length of 30 mm was machined using a wire electric discharge machining (EDM) that resulted in a notch 0.25 mm wide.

The test specimens were dynamically loaded in a three-point bend configuration by subjecting them to impact in a Dynatup 8100A drop weight tower. A schematic of the loading configuration is shown in Fig. 2. A tup mass of 200 kg and an impact velocity of 5 m/s were employed for all the experiments conducted. This dynamic impact of the precracked steel specimens results in deformation followed by fracture initiation. The dynamic deformation and fracture initiation process were monitored using high-speed infrared measurement of temperature and optical measurement of crack tip opening displacements. Details of the two experimental techniques are presented in the following sections.

2.2. Infrared temperature measurements

In this first series of experiments high-speed infrared diagnostics were introduced to study dynamic crack initiation for the first time in precracked ductile steel specimens impact loaded in a three point bend configuration. As the specimen was loaded, a high-speed HgCdTe infrared detector was employed to record the evolution of the temperature trace at a pre-determined location from the crack tip, as shown in Fig. 3. A Newtonian optical arrangement, illustrated in Fig. 3(a), employs a collecting mirror M_1 in conjunction with a plane mirror M_2 to map the area of interest on the specimen on to the infrared detector element. This results in a focused system such that there is a one-to-one mapping between the detector element and the area of interest on the specimen. Moreover, varying the object and image distances allows the magnification to be changed so that any desired area from the specimen can be mapped onto the detector element, which has a fixed size of $100 \times 100 \mu\text{m}$ square. The location of the area of interest on the specimen, which is essentially the area of temperature measurement, is situated well within the plastic zone that engulfs the

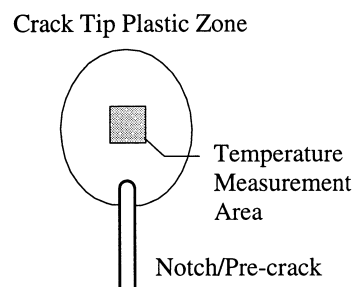
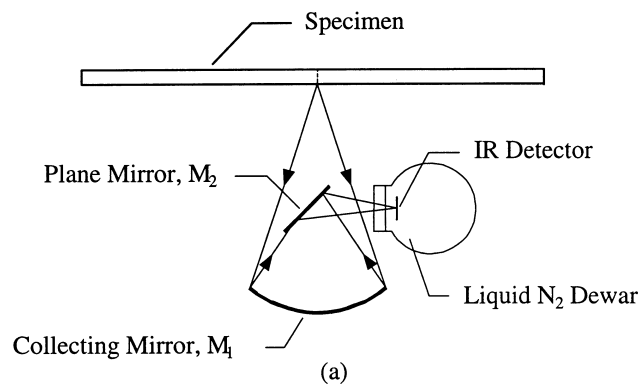


Fig. 3. Measurement of temperature variation in the vicinity of the dynamically loaded crack tip using an infrared detector. (a) Top view of specimen showing the infrared optical arrangement and (b) location of temperature measurement area on the specimen.

dynamically loaded crack tip, as shown in Fig. 3(b). If this temperature measurement is made at an appropriate location within the crack tip plastic zone surrounding the dynamically loaded crack tip, then, as it will be shown later, the history of the temperature trace can be directly related to the evolution of the dynamic value of the J -integral, $J^d(t)$.

2.3. Optical measurements of the crack tip opening displacement (CTOD)

In order to corroborate and evaluate the accuracy and applicability of the infrared temperature measurement technique to determine $J^d(t)$, optical measurements of the crack tip opening displacement (CTOD) were performed to measure the time history of the dynamic value of the J -integral, $J^d(t)$. The optical arrangement for the CTOD measurement, as illustrated in Fig. 4, employs a cavity dumped pulsed laser as the illumination source and a high-speed camera as the imaging system. A collimated laser beam is incident on the steel specimen, passes through the crack opening and is

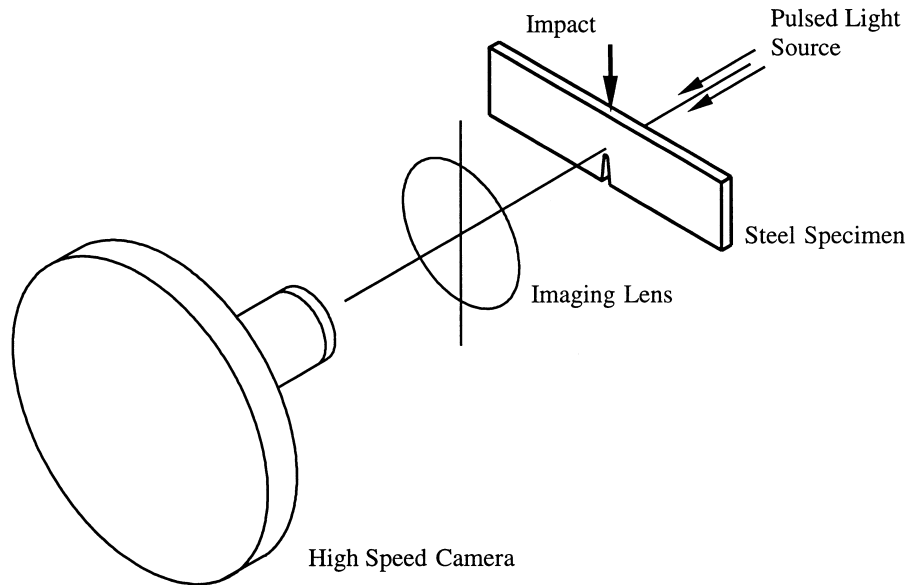


Fig. 4. Optical measurement of crack tip opening displacement (CTOD) using high speed photography.

imaged on to the film track of a rotating mirror type high-speed camera (Cordin Co., model 330A) with a maximum framing rate of 2 million/s. This results in the crack opening profile being photographed by the high-speed camera as the specimen undergoes dynamic deformation. The crack tip opening displacement is later measured directly from the recorded crack opening profiles. The camera recorded 80 frames of the dynamic event and was operated at an interframe time of $8.33 \mu\text{s}$ (120,000 frame/s). Individual frames were obtained by pulsing the laser light source (Spectra-Physics Argon-Krypton-ion laser, model 166-09; operating wavelength $\lambda = 514.5 \text{ nm}$ light) in a pulsed mode. The exposure time used in all experiments (i.e., the laser pulse duration) was 8 ns and the image was recorded on 35-mm black and white film (Kodak TMAX-400).

3. ANALYSIS PROCEDURE

The temperature measurements made in the vicinity of the dynamically loaded crack tip and the optical measurements of the crack tip opening displacement were analyzed to determine the time history of the dynamic value of the J -integral, $J^d(t)$. The analysis procedure involves the application of an appropriate asymptotic field that describes the crack tip stresses in an elastic-plastic material. The details of the analysis procedure are discussed in the following sections.

3.1. Asymptotic elastic–plastic crack tip field

Hutchinson (1968) and Rice and Rosengren (1968), collectively referred to as HRR, considered the case of a monotonically loaded stationary crack in a material described by a J_2 -deformation theory of plasticity and a power hardening relationship between the plastic strain ε_{ij}^p and stress σ_{ij} , and showed that the strain components in the crack tip region scale with the value of the J -integral. Within a small strain assumption, asymptotic solution of the elastic-plastic field equations in the crack tip region has the form

$$\varepsilon_{ij} \rightarrow \varepsilon_0 \left[\frac{J}{\sigma_0 \varepsilon_0 I_n r} \right]^{n/(n+1)} E_{ij}(n, \sigma) \quad (1)$$

$$\sigma_{ij} \rightarrow \sigma_0 \left[\frac{J}{\sigma_0 \varepsilon_0 I_n r} \right]^{1/(n+1)} \Sigma_{ij}(n, \theta) \quad (2)$$

as $r \rightarrow 0$. σ_0 is the tensile yield stress, ε_0 is the equivalent tensile yield strain, n is the hardening exponent, and the angular factors Σ_{ij} and E_{ij} depend on the mode of loading and the hardening exponent. The dimensionless quantity I_n is defined by Hutchinson (1968). The amplitude factor J is the value of Rice's J -integral (Rice, 1968). It has been suggested that, provided a one parameter representation of the crack tip fields remains valid, a condition for onset of crack growth is the attainment of a critical value of J .

3.2. Temperature rise associated with the HRR singular field

Consider an elastic–plastic isotropic homogeneous material with constant thermal conductivity. The heat conduction equation can be written as

$$k \nabla^2 \Theta - \alpha(3\lambda + 2\mu) \Theta_0 \dot{\varepsilon}_{kk}^e + \beta \sigma_{ij} \dot{\varepsilon}_{ij}^p = \rho c \dot{\Theta} \quad (3)$$

where, k is the thermal conductivity, Θ is the absolute temperature, α is the coefficient of thermal expansion, λ and μ are Lamé elastic constants, Θ_0 is the initial temperature, ε_{ij} and σ_{ij} are the Cartesian components of the strain and stress tensors, ρ is the mass density, and c is the specific heat. The quantity β is the fraction of plastic work rate density, $\dot{W}^p = \sigma_{ij} \dot{\varepsilon}_{ij}^p$, dissipated as heat. For the case of dynamic fracture in an elastic–plastic material we can neglect the thermo-elastic term, since $\dot{\varepsilon}_{ij}^e \ll \dot{\varepsilon}_{ij}^p$. Moreover, we can also assume the process to be sufficiently dynamic so that it can be approximated as being adiabatic. Hence, the heat conduction eqn (3) becomes

$$\frac{\beta}{\rho c} \sigma_{ij} \dot{\varepsilon}_{ij}^p = \dot{\Theta} \quad (4)$$

Substituting eqns (1) and (2) into eqn (4) we have

$$\dot{J}^d(t) = \frac{\rho c I_n}{\beta} \left(\frac{n+1}{n} \right) \frac{r}{\Sigma_{ij}(\theta, n) E_{ij}(\theta, n)} \dot{\Theta}(r, \theta, t) \quad (5)$$

On integrating eqn (5) with respect to time, t , we obtain

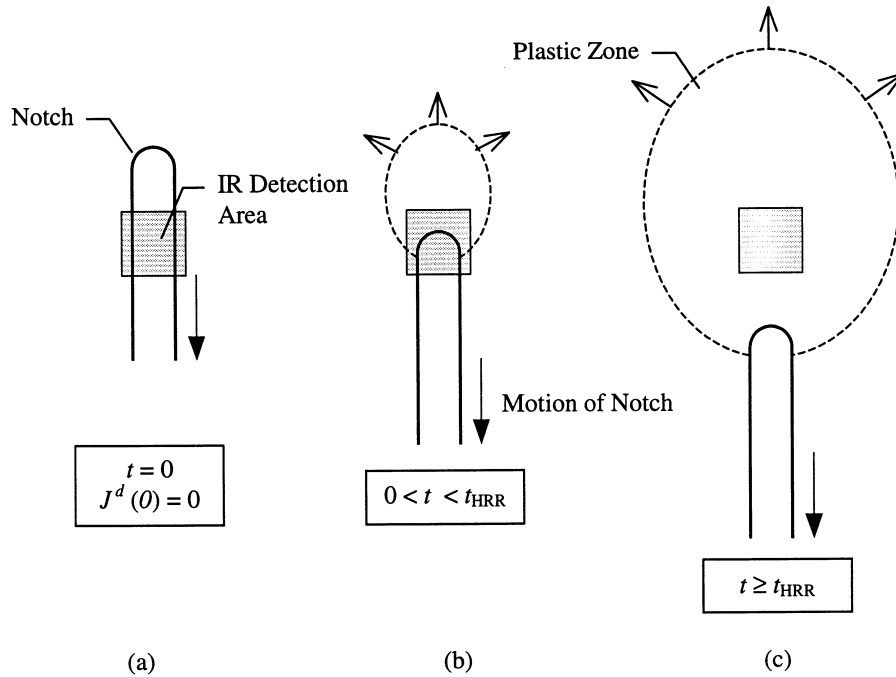


Fig. 5. Motion of the temperature sensing area relative to the crack tip as a function of time.

$$J^d(t) = \frac{\rho c I_n}{\beta} \left(\frac{n+1}{n} \right) \frac{r}{\sum_{ij}(\theta, n) E_{ij}(\theta, n)} [\Theta(r, \theta, t) - \Theta_0(r, \theta, t_0)] + J_0^d(t_0) \quad (6)$$

where $J_0^d(t_0)$ is the value of the J -integral at time $t = t_0$ and represents the integration constant. Equation (6) relates the time history of the dynamic value of the J -integral, $J^d(t)$, to the dynamic temperature rise in the vicinity of the crack tip.

It should be noted however that during the impact loading of the specimen the crack tip moves downward along with the motion of the impacting tup. This causes a relative motion between the crack tip and the area where the infrared temperature detector is focussed. This process is illustrated in Fig. 6. At the beginning of the

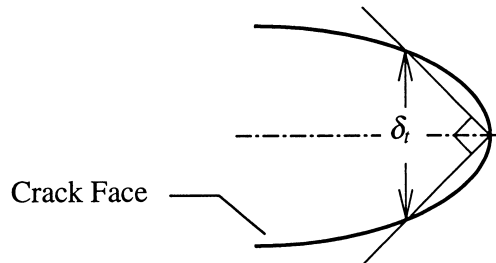


Fig. 6. Crack tip opening displacement defined on the basis of 90° intercepts (Shih, 1981).

experiment (pre-impact) the temperature detector is focussed at an area below the crack tip. During the post-impact loading and deformation process the crack tip moves downwards while the location of infrared temperature detection remains stationary, as shown in Fig. 5. Thus, it is only at some finite time, $t = t_{\text{HRR}}$, that the infrared detection area is well within the crack tip plastic zone and temperature is sensed in a zone characterized by the HRR singular field. This implies that eqn (6) is strictly valid only for, $t \geq t_{\text{HRR}}$, and hence is expressed as,

$$J^d(t) = \frac{\rho c I_n}{\beta} \left(\frac{n+1}{n} \right) \frac{r(t)}{\Sigma_{ij}(\theta, n) E_{ij}(\theta, n)} [\Theta(r, \theta, t) - \Theta_0(r, \theta, t_0)] + J^d(t_{\text{HRR}}), \quad t \geq t_{\text{HRR}} \quad (7)$$

The value of the dynamic J -integral at time $t = t_{\text{HRR}}$ is estimated, as a first approximation, by assuming a linear variation of $J^d(t)$ from $t = 0$ to $t = t_{\text{HRR}}$. It should also be noted that now the radial distance between the temperature detection area and the crack tip is given as a function of time, $r = r(t)$, which is experimentally determined using high speed photography.

3.3. Crack tip opening displacement (CTOD) associated with the HRR singular field

Consider crack face opening as shown in Fig. 6. Then the CTOD is defined using the intersection of a 90° vertex with the crack flanks. This definition of CTOD was invoked by Shih (1981) to relate the J -integral to the value of the crack tip opening displacement using the HRR singularity field as

$$J = \frac{\sigma_0}{d_n(\varepsilon_0, n)} \delta \quad (8)$$

where, δ is the CTOD, J is the value of the J -integral, σ_0 is the yield stress and d_n is a material dependent dimensionless constant as defined by Shih (1981). For the case of a dynamically loaded crack eqn (8) becomes

$$J^d(t) = \frac{\sigma_0}{d_n(\varepsilon_0, n)} \delta^d(t) \quad (9)$$

where, $J^d(t)$ is the dynamic value of the J -integral and $\delta^d(t)$ is the dynamic value of the CTOD.

4. EXPERIMENTAL OBSERVATIONS AND RESULTS

4.1. Measurement of $J^d(t)$

Typical variations of temperature measured in the vicinity of the crack tip for a dynamically loaded Ni–Cr steel specimen are shown in Fig. 7. Traces from two nominally similar experiments are plotted. There are a few features in the temperature traces that merit elucidation. The initial oscillations in the signal are due to the fact that the temperature detection area is moving past the crack tip (as in Fig. 5(b)) while

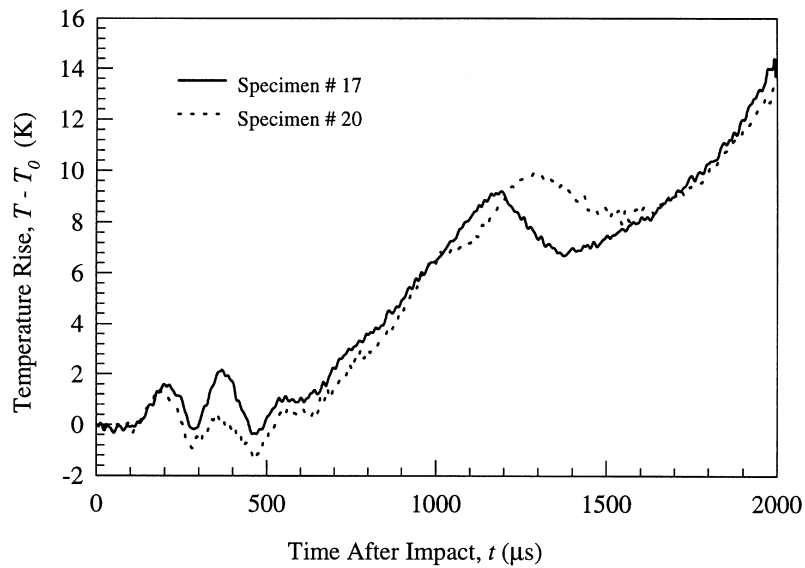


Fig. 7. Time history of the temperature variation in the vicinity of the dynamically loaded crack tip for a precracked Ni-Cr steel specimen subjected to three-point bend impact loading.

the specimen is undergoing initial structural oscillations resulting from impact. At about $550 \mu\text{s}$ after impact the temperature detection area is completely engulfed by the crack tip plastic zone and the transient temperature signal starts to increase steadily in a monotonic fashion. This increase remains steady until about $1200\text{--}1300 \mu\text{s}$ when a dip occurs in the temperature trace. It will be shown later, using strain gage instrumentation, that this dip corresponds to dynamic fracture initiation. Fracture initiation causes the specimen compliance to increase and thus results in a momentary decrease in the rate at which $J^d(t)$ increases, and possibly a drop in the value of $J^d(t)$. It should be noted that if the crack tip were stationary with respect to the temperature sensing area a decrease in the value of $J^d(t)$ would lead to elastic unloading and hence to thermoelastic cooling only. This would not cause any significant change in the temperature signal. However, in the present case the temperature detection area is continually moving away from the crack tip due to specimen motion. Therefore, since the temperature distribution exhibits r^{-1} dependence [eqn (6)], even a decrease in the rate at which $J^d(t)$ increases could lead to a drop in the temperature signal.

The transient temperature traces discussed above were analyzed using eqn (7) to determine the evolution of the instantaneous value of the J -integral, $J^d(t)$. The analysis procedure accounted for the relative motion of the temperature detection area with respect to the crack tip, $r = r(t)$, using high-speed photographic measurements of specimen (and crack tip) motion during the impact loading. Figure 8 shows a typical variation of $J^d(t)$ determined from infrared measurement of temperature in the vicinity of a dynamically loaded crack tip. This was the first time that a non-contact temperature measurement has been used to determine the time history of the dynamic J -integral, $J^d(t)$. Note that the values of $J^d(t)$ as shown in Fig. 8 will be valid only until

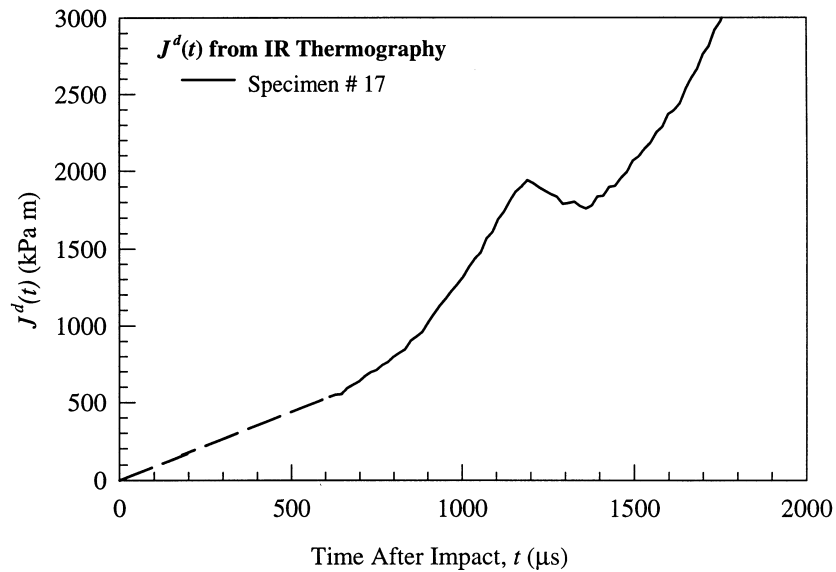


Fig. 8. Variation of the dynamic value of the J -integral as a function of time for Ni-Cr steel, as obtained from temperature measurement.

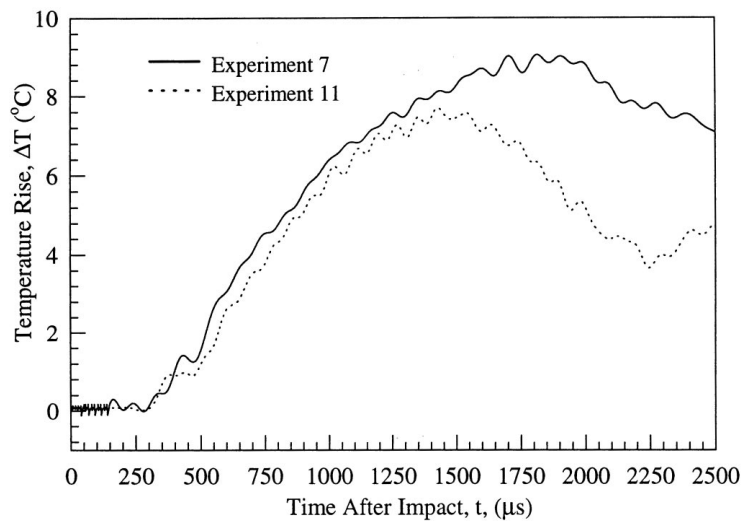


Fig. 9. Time history of the dynamic temperature variation in the vicinity of the dynamically loaded crack tip for a precracked 304 stainless steel specimen subjected to three-point bend impact loading.

the time of crack initiation, i.e. until the HRR asymptotic fields remain a good approximation of the crack tip fields.

Infrared thermography was also employed to study ductile failure of edge-cracked 304 stainless steel specimens subjected to three-point bend impact loading. Figure 9

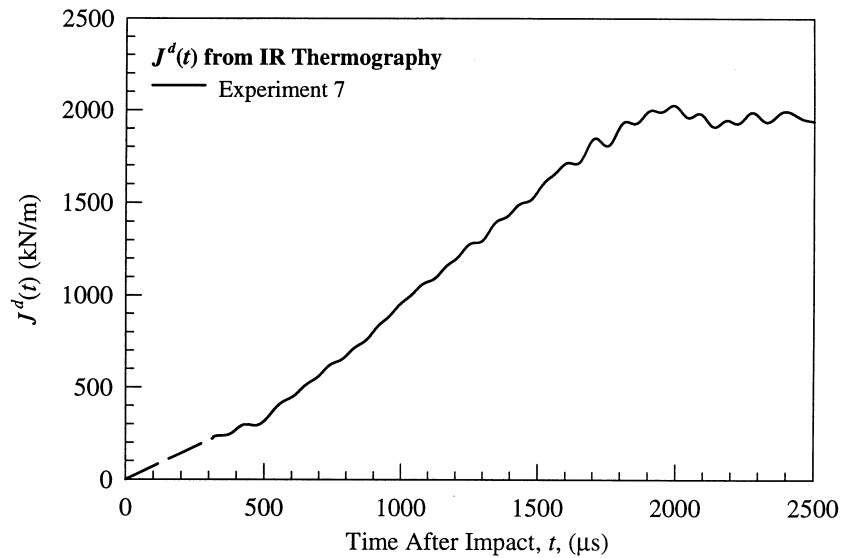


Fig. 10. Variation of the dynamic value of the J -integral as a function of time for 304 stainless steel, as obtained from temperature measurement.

shows typical variations of temperature measured in the vicinity of the dynamically loaded crack tip for a 304 stainless steel specimen. Traces from two nominally similar experiments are plotted. As shown in Fig. 9, the temperature traces begin to rise only after about 300 μs after impact, which coincides with the arrival of the plastic zone at the location where the temperature was being measured. A dip in the temperature traces occurred around 1500–1700 μs , which is associated with crack tip initiation. A typical time history of the dynamic J -integral, $J^d(t)$, as determined from the infrared temperature measurements is plotted in Fig. 10.

As discussed earlier, optical measurements of the crack tip opening displacements were made using a high-speed imaging system in order to validate the infrared thermography measurements of $J^d(t)$. Figure 11 shows a selected set of crack opening profiles obtained for three-point bend impact loading of an edge-cracked Ni–Cr steel specimen. The dynamic value of the CTOD, $\delta^d(t)$, was measured directly from these photographs using the 90° vertex intercept definition. Thereafter, time history of the dynamic value of the J -integral, $J^d(t)$, was determined from the CTOD variation in accordance with eqn (9). Figure 12 plots the time history of the dynamic J -integral, $J^d(t)$, as determined from measurements of the dynamic CTOD, $\delta^d(t)$. The figure also shows the variation of $J^d(t)$ as determined from infrared measurements of temperature. The excellent degree of correspondence between the two establishes the validity and accuracy of the infrared thermography technique to determine $J^d(t)$.

Optical measurements of the crack tip opening displacement were employed to determine the dynamic J -integral, $J^d(t)$, also for edge-cracked 304 stainless steel specimens subjected to three-point bend impact loading. Figure 13 shows the variation of $J^d(t)$ as determined from measurements of the dynamic CTOD, $\delta^d(t)$. Results

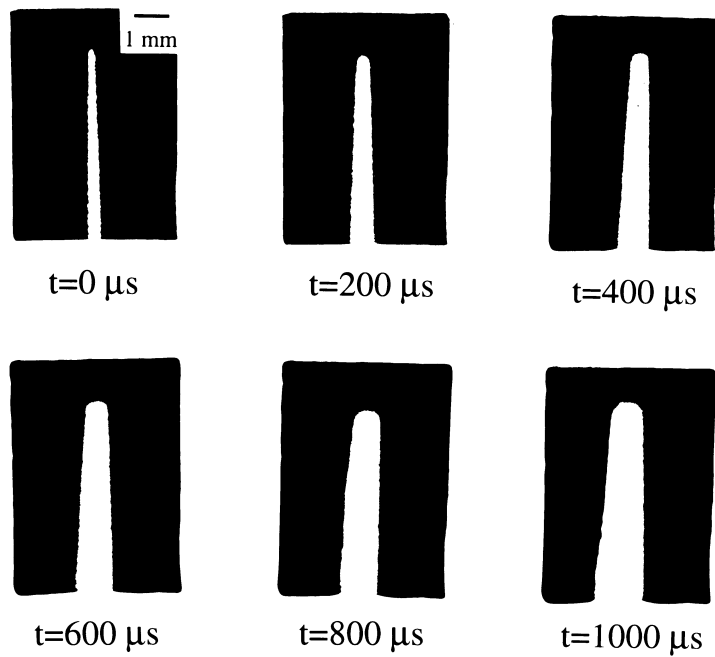


Fig. 11. Typical set of crack opening profiles obtained for a precracked Ni-Cr steel specimen subjected to three-point bend impact loading.

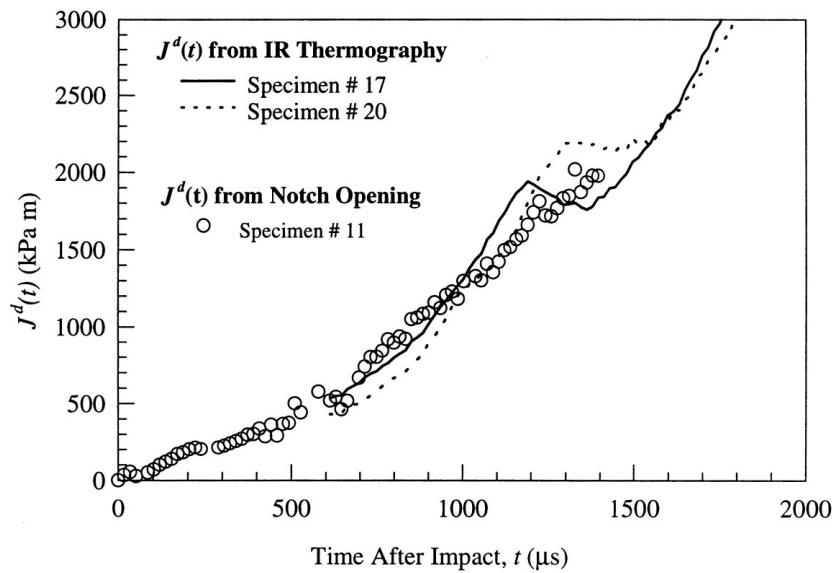


Fig. 12. Time history of the dynamic value of the J -integral as obtained from optical measurement of crack tip opening displacement and infrared measurement of temperature (Ni-Cr steel).

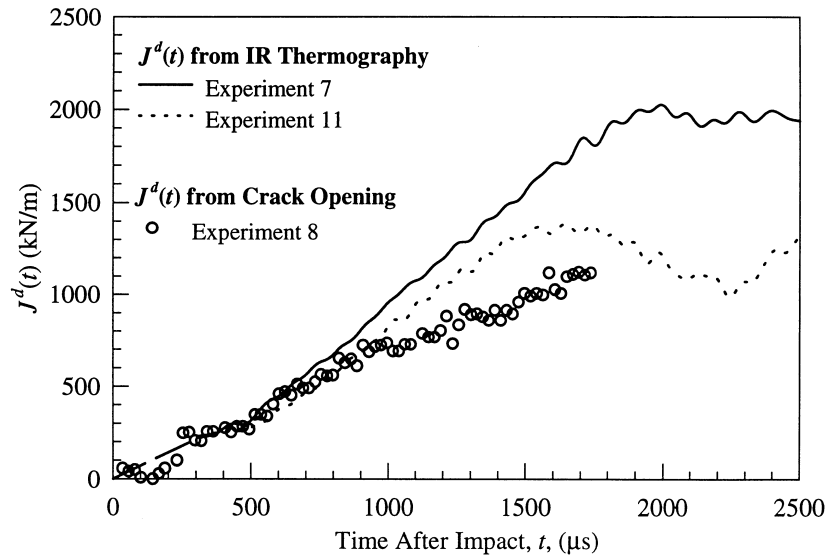


Fig. 13. Time history of the dynamic value of the J -integral as obtained from infrared measurement of temperature and optical measurement of crack tip opening displacement (304 stainless steel).

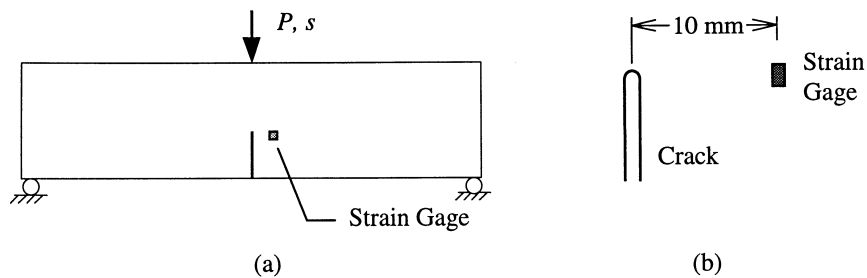


Fig. 14. Determination of fracture initiation during quasi-static loading of a precracked steel specimen. (a) Three-point bending loading configuration. (b) Location of strain gage with respect to crack tip.

obtained from infrared measurements of temperature are also plotted. There is excellent agreement between the two measurements for low values of $J^d(t)$. However, unlike the Ni–Cr case this correspondence breaks down for higher values of $J^d(t)$. This is due to the much higher deformations observed for the 304 stainless steel specimens. Equation (9), which relates the dynamic J -integral to the dynamic CTOD, is strictly valid only if the HRR singular field is an accurate representation of the stress and strain fields very close to the crack tip. However, for very large crack tip deformations this would not be the case and CTOD could not be expected to give an accurate estimation of the dynamic J -integral value. Nevertheless, away from the immediate vicinity of the crack tip the HRR singular field is still expected to hold and

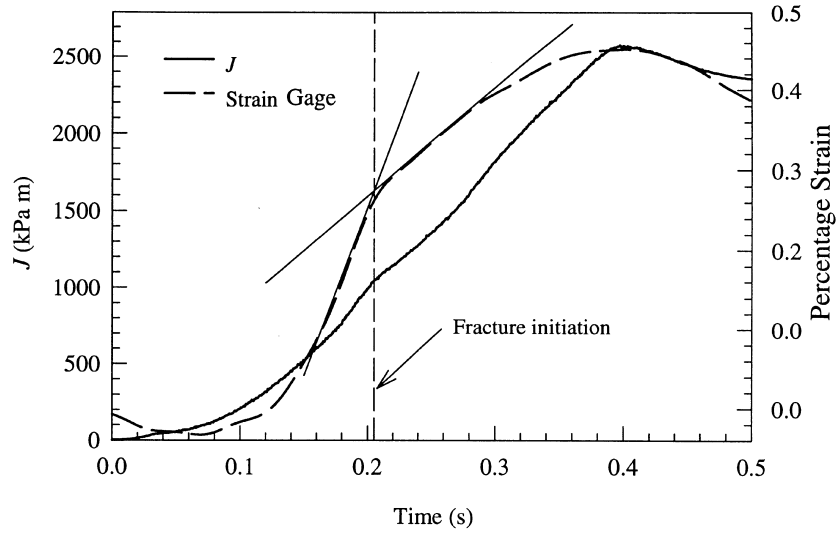


Fig. 15. Variation of the J -integral and strain gage signal during quasi-static three point bend loading of an edge cracked Ni-Cr specimen.

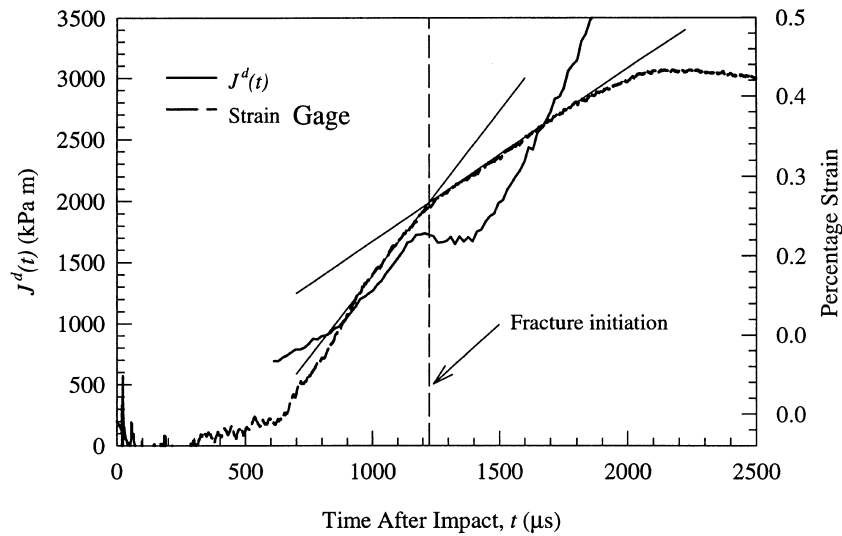


Fig. 16. Variation of the dynamic J -integral and strain gage signal during impact three-point bend loading of an edge cracked Ni-Cr specimen.

thus the infrared measurements of temperature would still provide a reasonable estimate of the dynamic J -integral value.

4.2. Identification of time of crack initiation

Identification of fracture initiation is a crucial step required to establish the dynamic fracture initiation toughness, $J^d(t_c) = J_c^d$, where $t = t_c$ is the time of fracture initiation.

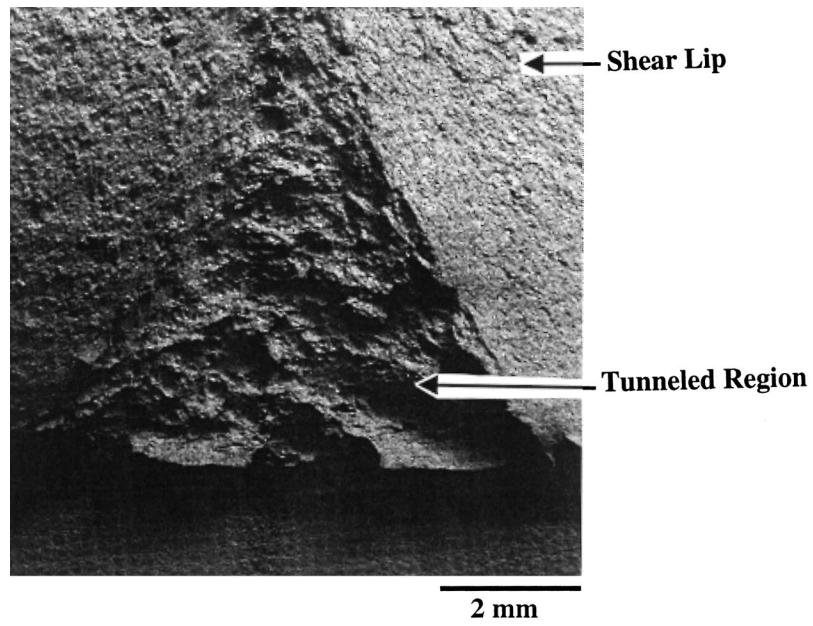


Fig. 17. A scanning electron micrograph of the fracture surface of Ni-Cr steel showing the tunneled region and the shear lip regions.

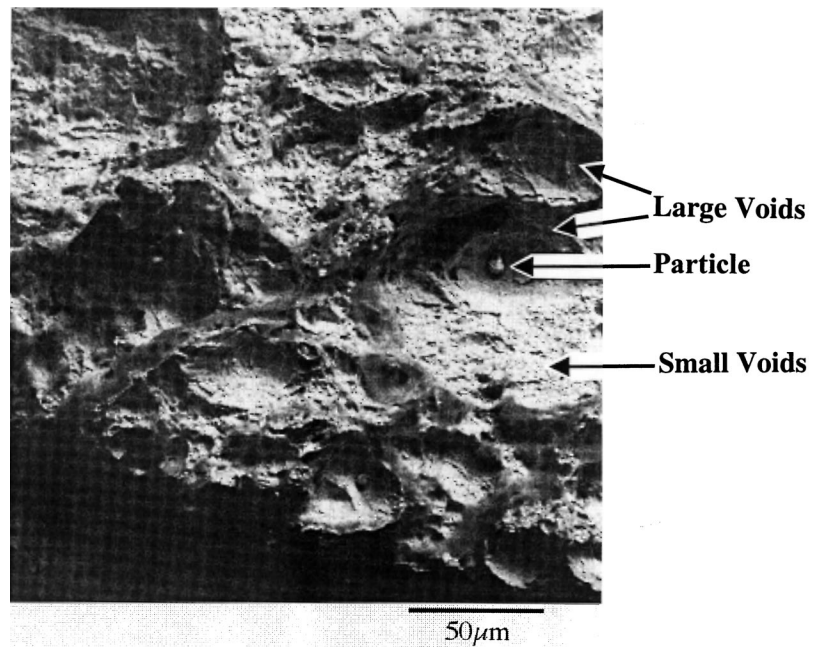


Fig. 18. SEM image of the tunneled region showing dual population of voids.

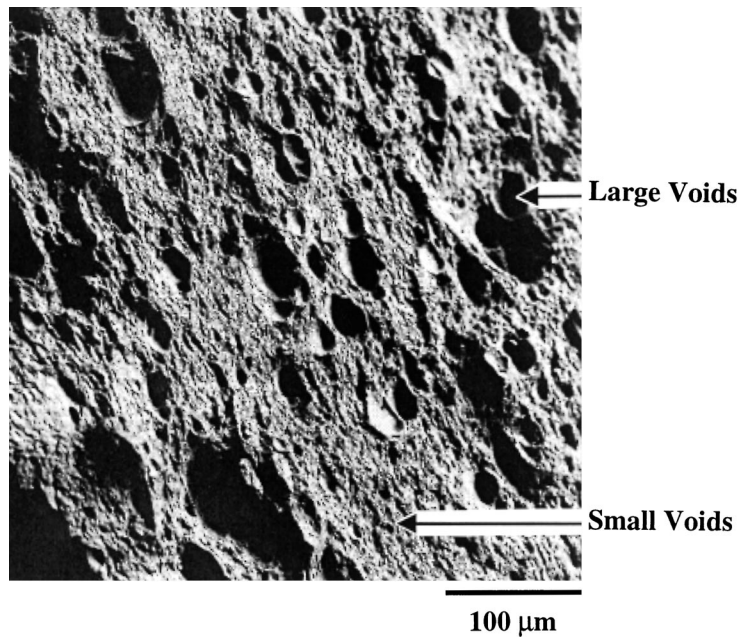


Fig. 19. SEM image of the shear lip region showing dual population of voids.

Strain gage instrumentation was employed to identify the fracture initiation event during dynamic deformation of the precracked steel specimens subjected to three-point bend impact loading (Couque, 1994). A strain gage located in the vicinity of the crack tip was employed to detect the change in specimen compliance that accompanies the fracture initiation event. The change in specimen compliance was reflected as a change in the rate at which the strain signal increases. As a first step, the strain gage technique was applied to identify the fracture initiation event in an edge-cracked specimen loaded quasi-statically in a three-point bend configuration. The advantage of quasi-static loading conditions is that the identification of fracture initiation can be corroborated with direct visual observation of the crack tip root. A schematic showing the loading arrangement and the strain gage location is given in Fig. 14. For this loading arrangement the value of the J -integral can be determined provided the load, P , and load point displacement, s , are known. Rice *et al.* (1973) have shown that

$$J = \frac{2}{tb} \int_0^\delta P ds \quad (10)$$

where b is the length of the uncracked ligament, t is the specimen thickness and δ is the load point displacement due to the presence of the crack. A typical variation of the value of the J -integral for quasi-static loading of an edge-cracked Ni–Cr steel specimen is shown in Fig. 15. The figure also shows the strain monitored by the strain gage employed to identify fracture initiation. The sudden change in slope of the

Table 3. *Fracture toughness as a function of loading rate for Ni–Cr steel and 304 stainless steel*

Ni–Cr steel		304 Stainless steel	
J_{crit}^d	J_{crit}^d	J_{crit}^d	J_{crit}^d
10 kN m ⁻¹ s ⁻¹	1080 kN m ⁻¹	8 kN m ⁻¹ s ⁻¹	1300 kN m ⁻¹
2500 kN m ⁻¹ s ⁻¹	1750 kN m ⁻¹	1300 kN m ⁻¹ s ⁻¹	1600 kN m ⁻¹

strain gage signal was identified as the fracture initiation event. This was confirmed simultaneously by direct visual observation of the crack tip root.

As a subsequent step, strain gages were employed to determine the fracture initiation event for dynamic three-point bend impact loading of a precracked Ni–Cr specimen. The strain gage location was selected to be the same as the quasi-static loading case. Figure 16 shows the variation of the strain as function of time during the impact loading of a precracked Ni–Cr steel specimen. The time history of the value of the dynamic J -integral, as determined by infrared thermography, is also shown in the same figure. As demonstrated in the figure, the fracture initiation event is clearly identified by the change in slope in the strain gage signal.

Table 3 lists the values of fracture initiation toughness, $J(t_c) = J_c$, obtained for quasi-static loading conditions and for dynamic loading. Fracture toughness values for both the steels are listed. The rate of loading at the time of fracture, $t = t_c$, is quantified in terms of the value of the rate of change of the J -integral. As can be seen from this data there is a significant increase in the value of the fracture toughness with increasing rate of loading for Ni–Cr steel. No such significant rise is observed for the 304 stainless steel.

4.3. *Micromechanisms of fracture initiation*

Ductile fracture in Ni–Cr and 304 stainless steels initiated in the form of tunneling in the center of the crack front followed by shear lip formation at the free surfaces. The failure process is dominated by void nucleation, growth and coalescence at the microstructural level. Figure 17 shows a scanning electron micrograph of the Ni–Cr fracture surface of a specimen loaded under dynamic conditions with tunnel and shear lip regions identified. Void formation begins in the center of the specimen due to the high constraint resulting from the prevailing plane strain conditions there, which leads to fracture initiation in the form of tunneling. These voids are nucleated at second phase particles in the microstructure. During the fracture process, these voids grow under the high crack tip stresses and eventually coalesce with each other and with the main crack. Figure 18 shows the voids and the particles that initiated these voids. Figure 18 also shows a much smaller void population filling up the regions between the larger voids. This points to the mechanism where the void coalescence takes place through the formation of void sheets consisting of a smaller void population. A similar mechanism appears to dominate the fracture process in the shear lip regions.

Figure 19 shows a detailed micrograph of the shear lip region. The elongated voids suggest that two mechanisms operated simultaneously in this region, i.e., void nucleation and growth and shear deformation. The distribution of smaller void population between the larger voids indicates that final failure again took place through the formation of void sheets.

5. SUMMARY

This study focuses on the development of a non-contact experimental technique to measure the history of the J -integral for dynamically loaded cracks in ductile solids. This technique utilizes infrared thermography for the first time to measure the temperature increase ahead of the dynamically deforming crack, which is subsequently related to the J -integral through HRR singular fields. The accuracy of this method is verified through an independent measurement of the dynamic J -integral, where high speed photography was used to measure the crack tip opening displacement (CTOD). A preliminary attempt has been made at understanding the micromechanisms of dynamic fracture initiation in ductile solids using scanning electron microscopy.

ACKNOWLEDGEMENTS

The authors would like to acknowledge the support of the Office of Naval Research under Grant No. N00014-95-1-0453 (Dr G. Yodder and Dr Y. D. S. Rajapakse, Scientific Officers) and of the Department of Energy under Grant No. De-FG03-95 ER14560 (Dr R. Goulard, Project officer). The authors are grateful to Dr D. M. Owen, Caltech, for his help in conducting the scanning electron microscopy and for other useful discussions.

REFERENCES

- Cho, K., Lee, S., Nutt, S. R. and Duffy, J. (1993) Adiabatic shear band formation during dynamic torsional deformation of an HY-100 steel. *Acta Metallurgica et Materialia* **41**, 923–932.
- Costin, L. S., Duffy, J. and Freund, L. B. (1977) Fracture initiation in metals under stress wave loading conditions. *Fast Fracture and Crack Arrest*. ASTM STP 627, American Society of Testing and Materials, pp. 301–318.
- Couque H. (1994) Effects of loading rate on the plane stress fracture toughness properties of an aluminum alloy. *Journal de Physique IV*, Colloque C8, Supplement au Journal de Physique III **4**, C8.747–C8.752.
- Douglas, A. S. and Suh, M. S. (1988) Impact fracture of a tough ductile steel. *Proceedings of the 21st ASTM National Fracture Symposium*. Annapolis, MD.
- Duffy, J. and Chi, Y. C. (1992) On the measurement of local strain and temperature during the formation of adiabatic shear bands. *Materials Science and Engineering* **A157**, 195–210.
- Hutchinson, J. W. (1968) Singular behavior at the end of a tensile crack in a hardening material. *Journal of Mechanics and Physics of Solids* **16**, 13–31.
- Li, Y. and Wang, Z. (1986) Higher order asymptotic field of tensile plane strain nonlinear crack problems. *Scientia Sinica (Series A)* **29**, 941–955.
- Nakamura, T. and Parks, D M. (1990) Three-dimensional crack tip fields in a thin ductile plate. *Journal of the Mechanics and Physics of Solids* **38**, 787–812.

- Narasimhan, R. and Rosakis, A. J. (1990) Three-dimensional effects near a crack tip in a ductile three-point bend specimen. I. A numerical investigation. *Journal of Applied Mechanics* **57**, 607–617.
- Needleman, A. and Tvergaard, V. (1987) An analysis of ductile rupture modes at a crack tip. *Journal of the Mechanics and Physics of Solids* **35**, 151–183.
- O'Dowd, N. P. and Shih, C. F. (1991) Family of crack tip fields characterized by a triaxiality parameter. I. Structure of fields. *Journal of the Mechanics and Physics of Solids* **39**, 989–1015.
- O'Dowd, N. P. and Shih, C. F. (1992) Family of crack tip fields characterized by a triaxiality parameter. II. Fracture applications. *Journal of the Mechanics and Physics of Solids* **40**, 939–963.
- Rice, J. R. (1968) A path independent integral and the approximate analysis of strain concentration by notches and cracks. *Journal of Applied Mechanics* **35**, 379–386.
- Rice, J. R. and Rosengren, G. F. (1968) Plane strain deformation near a crack tip in a power-law-hardening material. *Journal of the Mechanics and Physics of Solids* **16**, 1–12.
- Rice, J. R., Paris, P. C. and Merkle, J. G. (1973) Some further results on J -integral analysis and estimates. *Progress in Flaw Growth and Fracture Toughness Testing*. ASTM-STP 536, pp. 231–245.
- Rosakis, A. J. (1993) Two optical techniques sensitive to gradients of optical path difference: the method of caustics and the coherent gradient sensor (CGS). *Experimental Techniques in Fracture* pp. 327–425.
- Rosakis, A. J., Zehnder, A. T. and Narasimhan, R. (1988) Caustics by reflection and their application to elastic-plastic and dynamic fracture mechanics. *Optical Engineering* **27**(8), 596–610.
- Sharma, S. M. and Aravas, N. (1991) Determination of higher order terms in asymptotic elastoplastic crack tip solutions. *Journal of the Mechanics and Physics of Solids* **39**, 1043–1072.
- Sharpe Jr, J. R., Douglas, A. S. and Shapiro, J. M. (1988) Dynamic fracture toughness evaluation by measurement of C.T.O.D. Johns Hopkins Mechanical Engineering Report WNS-ASD-88-02.
- Shih, C. F. (1981) Relationships between the J -integral and the crack tip opening displacement for stationary and extending cracks. *Journal of the Mechanics and Physics of Solids* **29**, 305–326.
- Tippur, H. V., Krishnaswamy, S. and Rosakis, A. J. (1991) A coherent gradient sensor for crack tip measurements: analysis and experimental results. *International Journal of Fracture* **48**, 193–204.
- Yang, S., Chao, Y. J. and Sutton, M. A. (1993) Complete theoretical analysis for higher-order asymptotic terms and the HRR zone at a crack tip for mode I and mode II loading of a hardening material. *Acta Mechanica* **98**, 79–98.
- Zehnder, A. T., Rosakis, A. J. and Krishnaswamy, S. (1990) Dynamic measurement of the J -integral in ductile metals: comparison of experimental and numerical techniques. *International Journal of Fracture* **42**, 209–230.